

Enhanced BPINN Training Convergence in Solving General and Multi-scale Elliptic PDEs with Noise

Yilong Hou^{a,1}, Xi'an Li^{b,c,1,*}, Jinran Wu^d, You-Gan Wang^{e,*}

^aUniversity of California at Berkeley, CA, USA

^bCeyear Technologies Co., Ltd, Qingdao 266555, China

^cShandong University, Qingdao 266237, China

^dThe University of Queensland, St Lucia 4072, Australia

^eGuangdong University of Finance and Economics, Guangzhou 510320, China

Abstract

Bayesian Physics Informed Neural Networks (BPINN) have attracted considerable attention for inferring the system states and physical parameters of differential equations according to noisy observations. However, in practice, Hamiltonian Monte Carlo (HMC) used to estimate the internal parameters of the solver for BPINN often encounters these troubles including poor performance and awful convergence for a given step size used to adjust the momentum of those parameters. To address the convergence of HMC for the BPINN method and extend its application scope to multi-scale partial differential equations (PDE), we develop a robust multi-scale BPINN (dubbed MBPINN) method by integrating multi-scale deep neural networks (MscaledNN) and the BPINN framework. In this newly proposed MBPINN method, we reframe HMC with Stochastic Gradient Descent (SGD) to ensure the most “likely” estimation is always provided, and we configure its solver as a Fourier feature mapping-induced MscaledNN. This novel method offers several key advantages: (1) it is more robust than HMC, (2) it incurs less computational cost than HMC, and (3) it is more flexible for complex problems. We demonstrate the applicability and performance of the proposed method through some general Poisson and multi-scale elliptic problems in one and two-dimensional Euclidean spaces. Our findings indicate that the proposed method can avoid HMC failures and provide valid results. Additionally, our method is capable of handling complex elliptic PDE and producing comparable results for general elliptic PDE under the case of lower signal-to-noise rate. These findings suggest that our proposed approach has great potential for physics-informed machine learning for parameter estimation and solution recovery in the case of ill-posed problems.

Keywords: Bayesian-PINN, Multi-scale, Noisy observations, Convergence, Optimization, HMC
2010 MSC: 65F10, 65F50

1. Introduction

Partial differential equations (PDE) have extensive applications across various fields, as they model the physical properties and behaviors of complex systems. The parameters within these PDEs often represent key physical properties of the system under study [1]. To estimate these parameters or recover the solution based on observations and limited constraints, which can provide insights into the underlying physical phenomena [2]. In the context of well-posed problems, physics-informed neural networks (PINN) have demonstrated significant success in accurately estimating these parameters. However, in ill-posed problems,

*Corresponding author.

Email addresses: yilong.hou@berkeley.edu (Yilong Hou), lixian9131@163.com (Xi'an Li^b), wujrtudou@gmail.com (Jinran Wu^d), ygwang2012@gmail.com (You-Gan Wang^e)

¹These authors contributed equally to this work.

where the observations may be noisy or incomplete, the traditional numerical solvers often fail to provide reliable solutions [2]. To address these challenges, statistical and machine learning tools, such as regularizers, are employed to handle the ill-posed inverse problems by selecting or weighting variables [3, 4]. Bayesian statistics, as a natural regularization approach, has found numerous applications in dealing with noisy and high-dimensional data [5]. By integrating Bayesian statistics with PINN, some researchers have proposed robust methodologies for estimating parameters from real-world observational data in linear or nonlinear systems, thereby enhancing the accuracy and reliability of the analysis [6–8].

1.1. Bayesian PINN

In terms of the solution for the inverse problem governed by PDE, to improve the capacity of PINN for separating the system states and the noise from real noisy observation, we need to estimate well the internal parameters of PINN and system parameters based on those observations. Bayesian statistics offers effective inference methods for noisy and incomplete data [9]. By treating the parameters of PINN as random variables instead of unknown deterministic values, the Bayesian approach ultimately provides a distribution conditioned on observations as the inference of these parameters. When seeking a point estimate, such as the estimation of PINN parameters, Bayesian methodology regularizes the parameters so that useful parameters receive more weight, thereby controlling the error [5].

Consequently, Bayesian PINN is proposed using a Bayesian framework to estimate PINN parameters. Considering noise sampled from mean zero, i.i.d. normal distributions, BPINN uses Bayesian statistics as the estimation method and treats the likelihood accordingly. Finally, it employs Hamiltonian Monte Carlo (HMC) or variational inference (VI) for posterior sampling. This framework successfully quantifies uncertainty and improves predictions in noisy environments.

1.2. HMC and VI

The prior of BPINN can be assumed to be a Gaussian Process with mean 0 as the number of parameters goes to infinity [10, 11], but the distribution of the posterior is generally complicated and non-Gaussian due to the nonlinear nature of neural networks. Since the posterior distribution has no analytical expressions for the mean or the variance, they could only be approximated. There are generally two ways of approximating the posterior distribution, which are the HMC method and the VI method.

The HMC method is an enhancement of the Markov Chain Monte Carlo (MCMC) method. The new step of HMC is generated by solving the Hamiltonian system instead of a random walk in MCMC, but the acceptance procedure of each new step remains the same [12–14]. HMC is more efficient than MCMC by higher acceptance rate, but the computational cost remains high [1].

VI assumes that the posterior distribution belongs to a family of parameterized distributions. In other words, VI uses functions with a different parameterization to approximate the posterior distribution. By updating the parameters from this different parameterization, VI minimizes the KL divergence between the posterior distribution and its approximation. VI considers the optimal solution of this deterministic optimization problem as the best approximation of the posterior distribution [6, 15].

This paper chooses HMC over VI for theoretical and practical reasons. Theoretically, VI is projecting the posterior distribution onto a new function class which is usually assumed to be the mean-field Gaussian approximation by the deep learning community [16, 17]. Therefore, VI does not offer the same theoretical guarantees as MCMC approaches. Practically, lots of papers show that HMC has better performance than VI. For example, in high-dimensional problems [6] showing HMC’s superiority over VI and challenges.

1.3. Objective

Since the establishment of BPINN, they have demonstrated remarkable performance in solving mathematical problems in scientific computations and engineering applications based on their great potential in integrating prior knowledge with data-driven approaches. For example, utilizing BPINN to quantify uncertainties in the predictions of physical systems modeled by differential equations [17, 18], inverse problems [1, 19, 20], nonlinear dynamical system [8], etc.

After that, many efforts have been made to enhance the performance of BPINN are concluded as two aspects: the improvement of posterior sampling methods and the choice of NN-solver. In terms of the sampling strategy, one approach is to reduce the computational cost of the MCMC method [21, 22], and the other approach is to breach the gap between MCMC and VI through a partial-based VI approach. In the context of BPINN, methods like Stein Variational Gradient Descent (SVGD) [23] and Ensemble Kalman inversion (EKI) [1, 24, 25] has been proposed for sparse and noisy data. In terms of the latter one, the authors in [7] reconstructed the solver of PINN by extending the output pipelines and ensembled the multiple outputs at the same point to calculate statistical properties, then imposed any prior knowledge or assumptions regarding the uncertainty of the data. A Generative Adversarial Networks model is configured as the solver of BPINN (BPI-GAN) to learn flexible low-dimensional functional priors, e.g., both Gaussian and non-Gaussian processes, then BPI-GAN is easy to apply to big data problems by enabling mini-batch training using stochastic HMC or normalizing flows [26]. To robustly address multi-objective and multiscale problems, a novel methodology for automatic adaptive weighting of Bayesian Physics-Informed Neural Networks, which automatically tunes the weights by considering the multitask nature of target posterior distribution[27].

In practice, we found out that HMC is sensitive to the step size of updating parameters and sometimes does not converge to a stable distribution. The step size is used to adjust the momentum in the Hamiltonian system. When this step size is too large, the sum of the log-likelihood of the parameters goes to infinity and the algorithm breaks down. However, there are no explicit standards for the measure of step size. That is to say, one certain step size may work for a PDE, but fail for a different PDE. And even for the same PDE, changing the step size could make a huge impact on the performance of BPINN.

Additionally, as in the aforementioned BPINN methods, the solver is configured as a vanilla deep neural networks (DNN) model, then their performance will be limited by the spectral bias (or called frequency preference) of DNN and they may encounter some dilemmas for addressing complex problems, such as recovering the solution of multi-scale PDEs from noisy data [28, 29]. Recently, a multi-scale DNN (MscaleDNN) framework has been developed to resolve the issue of DNN which easily captures the low-frequency component of target functions but hardly matches the high-frequency component. Furthermore, a random Fourier feature embedding consisting of sine and cosine is introduced to improve the capacity of DNN, it will mitigate the pathology of spectral bias and enable networks to learn high frequencies more effectively[29–32].

In this paper, we develop an enhanced BPINN method by embracing the multi-scale DNN into BPINN framework (dubbed MBPINN), and reconstruct its estimation method to address the convergence problems of HMC-driven BPINN (BPINN_HMC) by replacing the original HMC with Stochastic Gradient Descent (SGD). Compared to the classical BPINN_HMC, this new approach ensures point estimation of the parameters with significantly lower computational costs. Additionally, the Fourier feature mapping consisting is used to further improve the performance of MBPINN to address general and complex problems under different noise levels. We apply this method across various types of PDE problems, including linear and nonlinear Poisson equations as well as multi-scale elliptic PDEs. The newly proposed method demonstrates strong potential and robustness in the aforementioned scenarios.

The remaining parts of our work are organized as follows. In Section 2, we briefly introduce the formulation BPINN and its failure through an example of a multi-scale PDE. Section 3 provides our solutions for both of the problems mentioned in the last section, by introducing the methodology of MBPINN and reframing HMC with SGD. In Section 4, some scenarios of multi-scale and general Poisson PDEs are performed to evaluate the feasibility and effectiveness for our proposed method. Finally, some conclusions of this paper are made in Section 5.

2. Formulation and Failure of Classical BPINN

2.1. Formulation of BPINN

In this subsection, we briefly introduce the formulation of BPINNs first proposed in [6]. Given a d -dimensional domain Ω and its boundary $\partial\Omega$, let us consider the following system of parametrized PDEs:

$$\begin{aligned}\mathcal{N}_{\lambda}[u(\mathbf{x})] &= f(\mathbf{x}), & \mathbf{x} \in \Omega \\ \mathcal{B}[u(\mathbf{x})] &= g(\mathbf{x}), & \mathbf{x} \in \partial\Omega\end{aligned}\tag{2.1}$$

in which \mathcal{N}_λ stands for the linear or nonlinear differential operator with parameters λ , \mathcal{B} is the boundary operators. Generally, the sampling data of force term $f(\mathbf{x})$ and boundary function $g(\mathbf{x})$ may be disturbed by unanticipated noise for real applications. The available dataset \mathcal{D} composed by the collocation points and the corresponding evaluation of f and g for this scenario is given by

$$\mathcal{D} = \mathcal{D}_f \cup \mathcal{D}_g \quad (2.2)$$

with

$$\mathcal{D}_f = \left\{ \left(\mathbf{x}_f^{(i)}, \tilde{f}^{(i)} \right) \right\}_{i=1}^{N_f} \quad \text{and} \quad \mathcal{D}_g = \left\{ \left(\mathbf{x}_g^{(j)}, \tilde{g}^{(j)} \right) \right\}_{j=1}^{N_g}.$$

In which, the above observations are i.i.d Gaussian random variables, i.e.,

$$\begin{aligned} \tilde{f}^{(i)} &= f(\mathbf{x}_f^{(i)}) + \varepsilon_f^{(i)}, \quad i = 1, 2, \dots, N_f, \\ \tilde{g}^{(j)} &= g(\mathbf{x}_g^{(j)}) + \varepsilon_g^{(j)}, \quad j = 1, 2, \dots, N_g, \end{aligned} \quad (2.3)$$

where $\varepsilon_f = \{\varepsilon_f^{(1)}, \varepsilon_f^{(2)}, \dots\}$ and $\varepsilon_g = \{\varepsilon_g^{(1)}, \varepsilon_g^{(2)}, \dots\}$ are independent mean-zero Gaussian noise with given standard deviations τ_f and τ_g , respectively. Note that the size of the noise could be different among observations of different terms, and even between observations of the same terms in the PDE.

To recover the solution of (2.1) from noisy observations through the Bayesian approach, the BPINN starts from representing u with a surrogate model $u_{NN}(\mathbf{x}; \boldsymbol{\theta})$, where $\boldsymbol{\theta}$ is the vector of parameters in the surrogate model with a prior distribution $P(\boldsymbol{\theta})$. When the process of the Bayesian method meets the physics-informed neural networks, the architecture of BPINN is constructed and its surrogate model is configured as a general DNN. Mathematically, the DNN defines the following mapping

$$\mathcal{F} : \mathbf{x} \in \mathbb{R}^d \implies \mathbf{y} = \mathcal{F}(\mathbf{x}) \in \mathbb{R}^c \quad (2.4)$$

with d and c being the dimensions of input and output, respectively. In fact, the DNN function \mathcal{F} is a nested composition of sequential single linear functions and nonlinear activation functions, which is in the form of

$$\begin{cases} \mathbf{y}^{[0]} = \mathbf{x} \\ \mathbf{y}^{[\ell]} = \sigma \circ (\mathbf{W}^{[\ell]} \mathbf{y}^{[\ell-1]} + \mathbf{b}^{[\ell]}), \quad \text{for } \ell = 1, 2, 3, \dots, L \end{cases} \quad (2.5)$$

where $\mathbf{W}^{[\ell]} \in \mathbb{R}^{n_{\ell+1} \times n_\ell}$, $\mathbf{b}^{[\ell]} \in \mathbb{R}^{n_{\ell+1}}$ are the weights and biases of ℓ -th hidden layer, respectively, $n_0 = d$ and n_{L+1} is the dimension of output, and “ \circ ” stands for the elementary-wise operation. The function $\sigma(\cdot)$ is an element-wise activation function. We denote the output of a DNN by $\mathbf{y}(\mathbf{x}; \boldsymbol{\theta})$ with $\boldsymbol{\theta}$ representing the parameter set of $\mathbf{W}^{[1]}, \dots, \mathbf{W}^{[L]}, \mathbf{b}^{[1]}, \dots, \mathbf{b}^{[L]}$.

Consequently, with the physical constraints, Bayes’ theorem under the context of BPINN can be formulated as follows:

$$P(\boldsymbol{\theta}|\mathcal{D}) = \frac{P(\mathcal{D}|\boldsymbol{\theta})P(\boldsymbol{\theta})}{P(\mathcal{D})} \simeq P(\mathcal{D}|\boldsymbol{\theta})P(\boldsymbol{\theta}), \quad (2.6)$$

Then, the log-likelihood can be calculated as:

$$\log P(\mathcal{D}|\boldsymbol{\theta}) = \log P(\mathcal{D}_f|\boldsymbol{\theta}) + \log P(\mathcal{D}_g|\boldsymbol{\theta}), \quad (2.7)$$

with

$$P(\mathcal{D}_f|\boldsymbol{\theta}) = \prod_{i=1}^{N_f} \frac{1}{\sqrt{2\pi\tau_f^2}} \exp \left(-\frac{\left\| \mathcal{N}_\lambda \left[u_{NN} \left(\mathbf{x}_f^{(i)}; \boldsymbol{\theta} \right) \right] - \tilde{f}^{(i)} \right\|^2}{2\tau_f^2} \right) \quad (2.8)$$

and

$$P(\mathcal{D}_g|\boldsymbol{\theta}) = \prod_{j=1}^{N_g} \frac{1}{\sqrt{2\pi\tau_g^2}} \exp\left(-\frac{\|\mathcal{B}[u_{NN}(\mathbf{x}_g^{(j)}; \boldsymbol{\theta})] - \tilde{g}^{(j)}\|^2}{2\tau_g^2}\right). \quad (2.9)$$

where $\|\cdot\|$ is the 2-norm for a given matrix or vector throughout the paper.

So far, we have specified the posterior distribution of BPINN. However, obtaining an explicit solution is often intractable. A traditional approach to approximate the posterior is to use sampling methods, such as Markov Chain Monte Carlo (MCMC). For instance, Hamiltonian Monte Carlo (HMC) (see Appendix 5) utilizes Hamiltonian dynamics to propose candidate parameter sets, followed by an acceptance-rejection mechanism to approximate the posterior density. Another widely used approach is variational inference (VI), which approximates the posterior by selecting a distribution Q from a family of distributions \mathcal{Q} and optimizing it to minimize the Kullback-Leibler (KL) divergence between Q and the true posterior. This is typically achieved using a reparameterization trick, which allows efficient gradient-based optimization of the variational parameters. And the well-approximated posterior will be used to infer PDE's numerical solution.

2.2. Failure of BPINN

HMC-driven BPINN method (called BPINN_HMC) has shown its remarkable performance in solving general PDEs, as demonstrated in [6]. However, the convergence of the HMC algorithm appears to be problematic when we try to extend BPINN to solve more complex PDE problems. The main problems are: 1) BPINN occasionally struggles to capture the primary signal in cases with highly oscillatory behavior, 2) sometimes HMC does not converge and provide us an available result.

To illustrate these two problems, we here introduce a concrete example in the context of multiscale elliptic PDEs. Let us consider the following one-dimensional elliptic equation with a homogeneous Dirichlet boundary in $\Omega = [0, 1]$:

$$\begin{cases} -\frac{d}{dx} \left(A^\varepsilon(x) \frac{d}{dx} u^\varepsilon(x) \right) = f(x), \\ u^\varepsilon(0) = u^\varepsilon(1) = 0, \end{cases} \quad (2.10)$$

in which

$$A^\varepsilon(x) = \frac{1}{2 + \cos(2\pi x/\varepsilon)}, \quad (2.11)$$

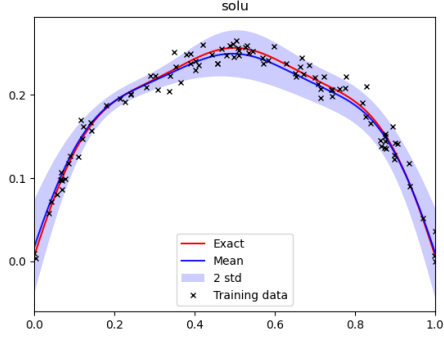
with $\varepsilon > 0$ being a small constant and $f(x) = 1$. Under these conditions, a unique solution is given by

$$u^\varepsilon(x) = x - x^2 + \varepsilon \left(\frac{1}{4\pi} \sin\left(2\pi \frac{x}{\varepsilon}\right) - \frac{1}{2\pi} x \sin\left(2\pi \frac{x}{\varepsilon}\right) - \frac{\varepsilon}{4\pi^2} \cos\left(2\pi \frac{x}{\varepsilon}\right) + \frac{\varepsilon}{4\pi^2} \right). \quad (2.12)$$

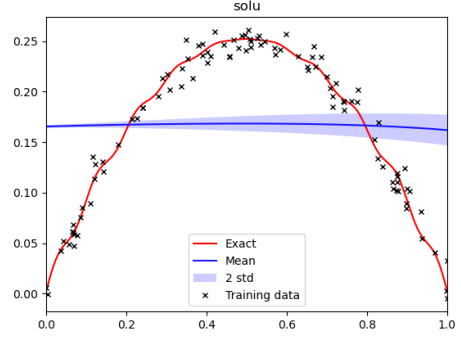
We employ the above BPINN_HMC method to solve the above problem when $\varepsilon = 0.5$ and $\varepsilon = 0.1$. For this study, we utilize 100 observations for system state and force side, respectively, in Ω to recover the solution of (2.10). Meantime, 1000 equidistant points are sampled in Ω to evaluate this method. The solver of BPINN_HMC comprises two hidden layers and each layer contains 30 hidden units. The activation function used in all hidden layers is the sine function, while the output layer is linear. To estimate the internal parameters of the BPINN, we run the BPINN_HMC method for 200 epochs and obtain the posterior distribution according to the results of the latter 150 epochs, the step number is 500 in each epoch and the step size used to update the internal parameters is fixed. Figures 1 – 3 demonstrate the performance of BPINN_HMC for both smooth case ($\varepsilon = 0.5$) and slight oscillation case ($\varepsilon = 0.1$) when the noise level is 0.01, 0.05 and 0.1, respectively. It reveals that this classical method will fail to capture the exact solution for other oscillation cases. Herein and thereafter, The symbol ‘—’ stands for the failure of HMC.

Furthermore, we perform BPINN_HMC with various step sizes (0.05, 0.001, 0.0005, 0.0001, 0.00001) to evaluate its robustness when the noise level is 0.01, 0.05 and 0.1, respectively. The results, as shown in Tables 1 and 2, indicate that the BPINN_HMC method will fail to converge and encounter errors when the step

size is large for different noise levels. This further underscores the limitations of the classical BPINN_HMC approach in dealing with both smooth and oscillation scenarios.

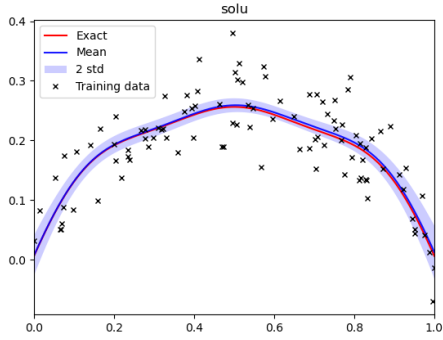


(a) u^ε for $\varepsilon = 0.5$

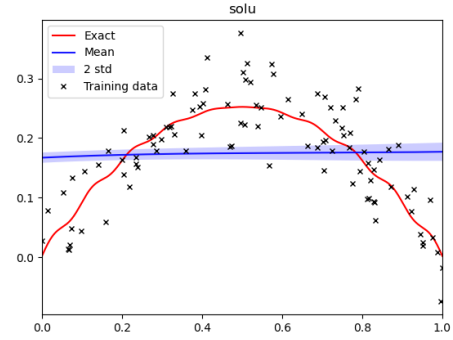


(b) u^ε for $\varepsilon = 0.1$

Figure 1: The predictions of BPINN_HMC and exact solution for $\varepsilon = 0.5$ and $\varepsilon = 0.1$ when noise level is 0.01, respectively.

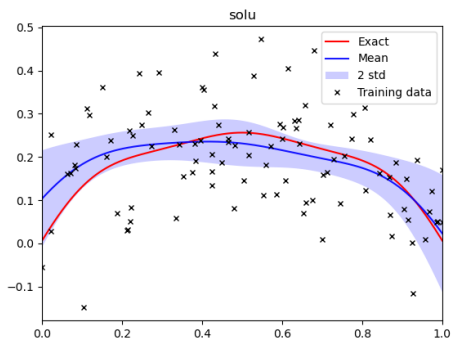


(a) u^ε for $\varepsilon = 0.5$

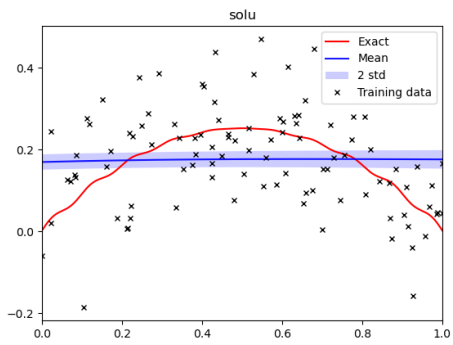


(b) u^ε for $\varepsilon = 0.1$

Figure 2: The predictions of BPINN_HMC and exact solution for $\varepsilon = 0.5$ when noise level is 0.05, respectively.



(a) u^ε for $\varepsilon = 0.5$



(b) u^ε for $\varepsilon = 0.1$

Figure 3: The predictions of BPINN_HMC and exact solution for $\varepsilon = 0.5$ when noise level 0.1, respectively.

Table 1: The performance of BPINN.HMC with different fixed step size when $\varepsilon = 0.5$.

Noise level	step size	0.01	0.005	0.001	0.0005	0.0001	0.00005	0.00001
0.01	Success/Failure	Failure	Failure	Failure	Failure	Failure	Failure	Success
	REL of solution	—	—	—	—	—	—	0.0242
0.05	Success/Failure	Failure	Failure	Failure	Failure	Success	Success	Success
	REL of solution	—	—	—	—	0.0220	0.0177	0.2567
0.1	Success/Failure	Failure	Failure	Failure	Failure	Success	Success	Success
	REL of solution	—	—	—	—	0.0543	0.1594	0.3204

Table 2: The performance of BPINN.HMC with different fixed step size when $\varepsilon = 0.1$.

Noisem level	step size	0.01	0.05	0.001	0.0005	0.0001	0.00005	0.00001
0.01	Success/Failure	Failure	Failure	Failure	Failure	Failure	Failure	Success
	REL of solution	—	—	—	—	—	—	0.3929
0.05	Success/Failure	Failure	Failure	Failure	Failure	Failure	Success	Success
	REL of solution	—	—	—	—	—	0.3958	0.3979
0.1	Success/Failure	Failure	Failure	Failure	Failure	Success	Success	Success
	REL of solution	—	—	—	—	0.4018	0.4016	0.3966

In addition, we perform the BPINN with different setups of the hyperparameters such as the number of sampled points and burn-in points as well as the network size, but we still cannot obtain a satisfactory result. Based on the above observation, it is necessary to probe into the misconvergence of HMC and develop new techniques to improve the accuracy and robustness of the BPINN method.

In this sensoria, the HMC may fail to converge in complex inference problems due to several challenges inherent to the posterior distribution and the algorithm’s mechanics. First, HMC struggles with multimodal posterior distributions, where the parameter space contains multiple isolated regions of high probability. HMC generates samples by simulating the dynamics of a particle moving through the parameter space, and each HMC chain represents a sequence of such samples. In such cases, a single HMC chain can become trapped in one mode, unable to explore the entire posterior within a reasonable time [33]. Second, The high dimensionality of the parameter space exacerbates the difficulty of effective sampling, as high-dimensional posteriors often exhibit strong correlations and complex geometric structures that hinder efficient exploration by the Markov chains. This can lead to poor mixing and slow transitions between regions of high probability. As shown in Figure 12, the point-wise error for HMC displays significant variability, with noticeable error peaks indicating regions where the posterior distribution is not well captured. These limitations highlight the difficulty of using HMC in high-dimensional settings, especially when the posterior geometry complicates sampling and convergence. Additionally, high curvature in certain areas of the posterior can cause numerical instability in HMC’s leapfrog integrator, further impeding convergence. For example, as shown in Appendix 5, the momentum is updated using the *param_grad* function, where momentums of the parameters are calculated. Poorly scaled gradients or an imbalanced parameter space often lead to excessively large momentum values, which propagate through the leapfrog updates, causing the likelihood of the parameters to explode to infinity. This instability is exacerbated in high-dimensional or complex, non-linear problems, where the posterior distribution exhibits sharp gradients or strong correlations. These challenges emphasize the importance of careful tuning of HMC hyperparameters, such as step size and trajectory length, which become increasingly sensitive under such conditions. As a result, HMC may fail to provide a representative sample of the posterior, leading to biased estimates and unreliable inference.

3. Methodology

3.1. SGD Reframed HMC method

In this section, to avoid the convergence failure of classic HMC, we would like to use SGD to reframe the existing method. Unlike HMC, where the entire posterior distribution of the parameters is modeled, we aim to find the set of parameters that are most “likely”, as this procedure guarantees a solution. Notice that, in each step of HMC, a likelihood is calculated for a set of parameters and is used to determine whether this step will be accepted. Finally, all accepted steps form the empirical posterior distribution. The algorithm of HMC is as in Appendix 5.

Through the HMC algorithm Appendix 5, we could see that each set of parameters is considered as a sample from the numerator of the posterior distribution, also referred to as the kernel function of BPINN. We would like to define the most “likely” set of parameters as the set that maximized the kernel function. Thus, by finding the most “likely” set of parameters, we mean seeking to find the maximum of the true distribution by viewing the inverse of the likelihood as the loss. The larger the likelihood, the smaller the loss. This turns the problem into an optimization problem, and we use typical stochastic gradient descent (SGD) to find the optimum.

Algorithm 1 Adam optimization method

Require: Stepsize α and Exponential decay rates for the moment estimates $\beta_1, \beta_2 \in (0, 1]$

Require: Stochastic objective function $f(\theta)$ with parameters θ

Input: Initialize the parameter vector $\theta_0 \neq \mathbf{0}$, the 1^{st} moment vector $\mathbf{m}_0 = \mathbf{0}$, the 2^{nd} moment vector $\mathbf{v}_0 = \mathbf{0}$ and timestep $t = 0$

```

1: while  $\theta_t$  not converged do
2:    $t = t + 1$ 
3:    $\mathbf{g}_t = \nabla_{\theta} f_t(\theta_{t-1})$ 
4:    $\mathbf{m}_t = \beta_1 \cdot \mathbf{m}_{t-1} + (1 - \beta_1) \cdot \mathbf{g}_t$ 
5:    $\mathbf{v}_t = \beta_2 \cdot \mathbf{v}_{t-1} + (1 - \beta_2) \cdot \mathbf{g}_t \odot \mathbf{g}_t$ 
6:    $\widehat{\mathbf{m}}_t = \mathbf{m}_t / (1 - \beta_1^t)$ 
7:    $\widehat{\mathbf{v}}_t = \mathbf{v}_t / (1 - \beta_2^t)$ 
8:    $\theta_t = \theta_{t-1} - \alpha \cdot \widehat{\mathbf{m}}_t / (\sqrt{\widehat{\mathbf{v}}_t} + \varepsilon)$ 
9: end while
10: return  $\theta_t$ 

```

3.2. MBPINN

In this section, the unified architecture of MBPINN is proposed to estimate the parameters and recover the solution of PDEs according to the given observation data with unexpected noise by embracing the vanilla BPINN method with Fourier-induced MscaledDNN.

In terms of the BPINN method, its solver is configured as a general DNN. As we are aware, a general DNN model is capable of providing a satisfactory solution for low-complexity problems but will encounter troublesome difficulty in solving complex problems such as multi-scale PDEs. From the perspective of spectral bias or frequency preference, the DNN is typically efficient for fitting objective functions with low-frequency modes but inefficient for high-frequency functions. Therefore, the PINN method have the same phenomenon, it will have an adverse impact for the performance of BPINN. Neural Tangent Kernel (NTK) theory has been used to model and understand the behavior of DNN[30].

Recently, a MscaledDNN architecture has been proposed based on the intrinsic property of DNN to mitigate the pathology of DNN by converting original data to a low-frequency space [34–37]. According to the NTK theory, the authors in [30] developed a random Fourier feature mapping (FFM) induced Physics-informed neural networks to enhance the robustness and accuracy of conventional PINN for solving multi-

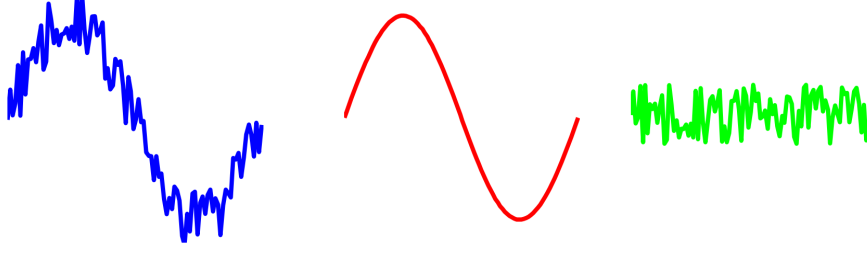


Figure 4: The decomposition of multi-scale function. Left: Original function, Middle: Coarse part, Right: Oscillation part

scale PDEs, this new framework is another type of MscaleDNN. The FFM is expressed as follows

$$\zeta(\mathbf{x}) = \begin{bmatrix} \cos(\pi\Lambda\mathbf{x}) \\ \sin(\pi\Lambda\mathbf{x}) \end{bmatrix}$$

where Λ is a transmitted matrix that is consistent with the dimension of input data and the number of neural units for the first hidden layer in DNN, and its elements are sampled from an isotropic Gaussian distribution $\mathcal{N}(0, \xi)$ with $\xi > 0$ is a user-specified hyper-parameter. Numerical simulations demonstrated the heuristic sinusoidal mapping of input will enable DNN to efficiently fit higher frequency functions. Moreover, the authors in [32] proposed a modified FFM that keeps the original independent variables as the input to balance the ability of DNN and PINN for dealing with low frequencies and high frequency components. In this paper, we modify this strategy by utilizing a linear transformation for the inputs data, it is

$$\zeta(\mathbf{x}) = \begin{bmatrix} \text{Lin}(\mathbf{x}) \\ \cos(\pi\Lambda\mathbf{x}) \\ \sin(\pi\Lambda\mathbf{x}) \end{bmatrix}$$

where $\text{Lin}(\mathbf{x}) = \mathbf{W}_{lin}\mathbf{x} + \mathbf{b}_{lin}$ with \mathbf{W}_{lin} being the weight matrix and \mathbf{b}_{lin} being the bias vector.

Hence, we can improve the capacity of BPINN by embracing the multi-scale DNN with the above modified FFM, called it as MBPINN method. A schematic diagram of MscaleDNN with multiple modified FFM pipelines is described as follows.

$$\begin{aligned} \hat{\mathbf{x}} &= \mathbf{\Lambda}_n \mathbf{x}, \quad n = 1, 2, \dots, N, \\ \zeta_n(\mathbf{x}) &= \begin{bmatrix} \text{Lin}(\mathbf{x}) \\ \cos(\pi\hat{\mathbf{x}}) \\ \sin(\pi\hat{\mathbf{x}}) \end{bmatrix}, \quad n = 1, 2, \dots, N, \\ \mathbf{F}_n(\mathbf{x}) &= \mathcal{FCN}(\zeta_n(\mathbf{x})), \quad n = 1, 2, \dots, N, \\ \mathbf{NN}(\mathbf{x}) &= \mathbf{W}_O \cdot [\mathbf{F}_1, \mathbf{F}_2, \dots, \mathbf{F}_N] + \mathbf{b}_O, \end{aligned} \tag{3.1}$$

in which, \mathcal{FCN} stands for a fully connected neural network. \mathbf{W}_O and \mathbf{b}_O represent the weights and bias for the output layer of MscaleDNN, respectively.

For a given multi-scale PDE, the solution generally has the following coarse/fine decomposition, $u = u_c + u_f$, in which u_c contains the smooth part and u_f contains the fine details of the multi-scale solution u , respectively. Please see figure 4. Naturally, the force term f and the boundary constraint g may also be oscillating and could be decomposed as $f = f_c + f_f$ and $g = g_c + g_f$, respectively. Analogously, we have the collection set for governed equation and boundary constraint, i.e., $\mathcal{D}_f = \left\{ \left(x_f^{(i)}, \tilde{f}^{(i)} \right) \right\}_{i=1}^{N_f}$ and $\mathcal{D}_g = \left\{ \left(x_g^{(j)}, \tilde{g}^{(j)} \right) \right\}_{j=1}^{N_g}$. These observation are i.i.d Gaussian random variables and they have the following

formulations

$$\tilde{f}^{(i)} = f_c(x_f^{(i)}) + f_f(x_f^{(i)}) + \varepsilon_f^{(i)}, \quad x_f^{(i)} \in \mathcal{D}_f \text{ and } i = 1, 2, \dots, N_f, \quad (3.2)$$

$$\tilde{g}^{(j)} = g_c(x_g^{(j)}) + g_f(x_g^{(j)}) + \varepsilon_g^{(j)}, \quad x_g^{(j)} \in \mathcal{D}_g \text{ and } j = 1, 2, \dots, N_g. \quad (3.3)$$

As well as, the ε_f and ε_g are same as the aforementioned definitions in section 2.1.

Within the framework of MBPINN, the log-likelihood can be calculated as follows:

$$\log P(\mathcal{D}|\theta) = \log P(\mathcal{D}_f|\theta) + \log P(\mathcal{D}_g|\theta), \quad (3.4)$$

with

$$P(\mathcal{D}_f|\theta) = \prod_{i=1}^{N_f} \frac{1}{\sqrt{2\pi\tau_f^2}} \exp \left(-\frac{\|\mathcal{N}_\lambda[u_{NN}(x_f^{(i)}; \theta)] - \tilde{f}^{(i)}\|^2}{2\tau_f^2} \right) \quad (3.5)$$

and

$$P(\mathcal{D}_g|\theta) = \prod_{j=1}^{N_g} \frac{1}{\sqrt{2\pi\tau_g^2}} \exp \left(-\frac{\|\mathcal{B}[u_{NN}(x_g^{(j)}; \theta)] - \tilde{g}^{(j)}\|^2}{2\tau_g^2} \right). \quad (3.6)$$

If some additional observed data are available inside the interested domain, it is $\mathcal{D}_u = \left\{ (x_u^{(k)}, \tilde{u}^{(k)}) \right\}_{k=1}^{N_u}$ with $\tilde{u}^{(k)} = u_c(x_u^{(k)}) + u_f(x_u^{(k)}) + \varepsilon_u^{(k)}$, $k = 1, 2, \dots, N_u$, then a log-likelihood term indicating the mismatch between the predictions produced by MBPINN and the observations can be taken into account

$$P(\mathcal{D}_u|\theta) = \prod_{k=1}^{N_u} \frac{1}{\sqrt{2\pi\tau_u^2}} \exp \left(-\frac{\|u_{NN}(x_u^{(k)}; \theta) - \tilde{u}^{(k)}\|^2}{2\tau_u^2} \right) \quad (3.7)$$

where τ_f is the standard deviations for mean-zero Gaussian noise ε_u . At the end, we conclude the section with the schematic of the MBPINN architecture in Figure 5.

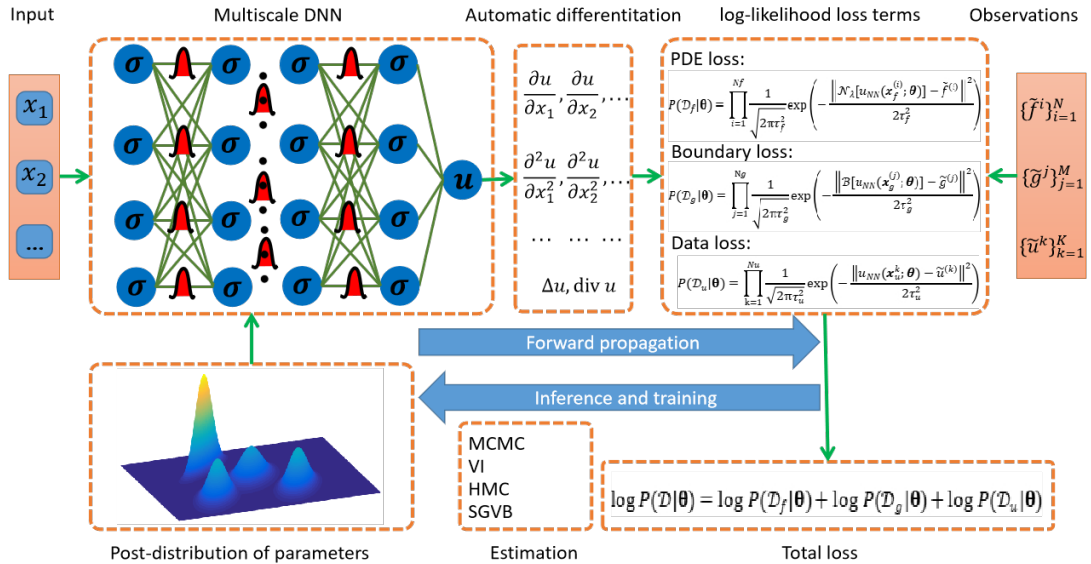


Figure 5: The semantic diagram for MBPINN to solve multi-scale PDEs with noise

4. Experiment

The goal of our experiments is to show that our MBPINN with SGD reframed HMC is indeed capable of approximating the analytical solution for given general and complex PDE based on observations with various noise levels. In addition, the BPINN method with a DNN model being its solver is introduced to serve as the baseline. Six types of compared methods are described in the following:

- *BPINN_HMC*: Its solver is a normal DNN model with the Sine function being the activation function for all hidden layers, while the output layer is linear. The approach of estimating its parameters is classical HMC [6].
- *BPINN_SGD*: Its solver is a normal DNN model with the Sine function being the activation function for all hidden layers, while the output layer is linear. The approach of estimating its parameters is SGD (Adam).
- *FF_MBPINN_HMC*: Its solver is an MscaleDNN model with an FFM pipeline, the activation function for the remainder hidden layers is chosen as Sine, while the output layer is linear. The approach to estimating its parameters is classical HMC.
- *FF_MBPINN_SGD*: Its solver is a MscaleDNN model with an FFM pipeline, the activation function for the remainder hidden layers is chosen as Sine, while the output layer is linear. The approach to estimating its parameters is SGD (Adam).
- *2FF_MBPINN_HMC*: Its solver is an MscaleDNN model with two FFM pipelines, the activation function for the remainder hidden layers is chosen as Sine, while the output layer is linear. The approach to estimating its parameters is classical HMC.
- *2FF_MBPINN_SGD*: Its solver is a MscaleDNN model with two FFM pipelines, the activation function for the remainder hidden layers is chosen as Sine, while the output layer is linear. The approach to estimating its parameters is SGD (Adam).

For comparison, we run HMC algorithm for 200 trajectories, then record the last 150 trajectories and obtain the posterior distribution. In each trajectory, the step number to update network's parameters is set as 500 and the step size is fixed. In addition, we perform the SGD (Adam) used in the above methods with a fixed learning rate for 20000 epochs and obtain the most 'likely' parameters of the FF_MBPINN_SGD and 2FF_MBPINN_SGD methods according to the final epoch's results. In our test, the step size or learning rate are set as 0.01, 0.005, 0.001, 0.0005, 0.0001, 0.00005 and 0.00001, respectively.

As for the observations, we generate them based on random sampling strategy (For example, Latin Hypercube Sampling (LHS)) in the interest domain. In which, LHS is a statistical method that provides a more randomized distribution of points, particularly useful for high-dimensional spaces, while ensuring boundary points are included and corresponding values are computed with noise. Finally, we add noise based on different noise levels. Noise level is defined by the constant times of a standard normal distribution. For example, the noise level of 0.1 means $0.1 * \mathcal{N}(0, 1)$. In addition, we utilize the signal-to-noise ration (SNR) to describe the influence of noise for solution, coefficient term and force size, respectively. It is

$$SNR = 10 \log \left(\frac{Ps}{Pn} \right)$$

where Ps and Pn stand for the signal power and noise power, respectively.

To quantitatively measure the performance of our model, we compute the point-wise Absolute Error (ABSE) and the Relative Error (REL) between the mean-predicted and the exact solutions. The ABSE is given by

$$ABSE = |\hat{u}(x'_i) - u^*(x'_i)|, \quad i = 1, 2, \dots, N'$$

and the REL is calculated as follows:

$$\text{REL} = \sqrt{\frac{\sum_{i=1}^{N'} |\hat{u}(x'_i) - u^*(x'_i)|^2}{\sum_{i=1}^{N'} |u^*(x'_i)|^2}},$$

where $\hat{u}(x'_i)$ denotes the mean-predicted solution at point x'_i , $u^*(x'_i)$ is the exact solution, and N' is the total number of evaluation points.

4.1. Performance of MBPINN for Solving 1-dimensional PDEs

Example 1. In this example, the problem setups are same as the section 2.2 and we solve this two-scale elliptic problem when $\varepsilon = 0.1$ by employing the aforementioned six methods that their solvers have two hidden layers and each layer has 30 units. In our test, we only disturb the observation of the solution with a mean-zero Gaussian distributed noise on 98 inner random sampled points and 2 boundary points. As for the observations of force term, 100 observations located randomly in Ω are disturbed with mean-zero Gaussian distributed noise. To approximate the solution, the standard deviation for Λ of MscaleDNN in FF_MBPINN is set as 5, the standard deviations for Λ_1 and Λ_2 of MscaleDNN in 2FF_MBPINN are set as 1 and 5, respectively. Moreover, in order to showcase the performance of our proposed method, the SNRs for solution and force side under various noise levels are listed in Table 3. We list and depict the related experiment results in Tables 4 – 6 and Figures 6 – 8, respectively.

Table 3: SNR of solution and force side under various noise level for Example 1.

Noise level	0.01	0.05	0.1
solution	24.527	12.181	5.008
force side	39.537	27.193	20.811

Table 4: REL of different method to solve Example 1 when the noise level is 0.01.

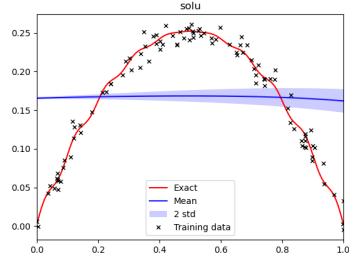
Initial step size(lr)	0.01	0.005	0.001	0.0005	0.0001	0.00005	0.00001
BPINN_HMC	—	—	—	—	—	—	0.3929
FF_MBPINN_HMC	—	—	—	—	—	—	—
2FF_MBPINN_HMC	—	—	—	—	—	—	—
BPINN_SGD	0.3931	0.3957	0.3854	0.3873	0.3953	0.3965	0.3943
FF_MBPINN_SGD	0.2132	0.0892	0.0083	0.0198	0.0174	0.0195	0.3014
2FF_MBPINN_SGD	0.3125	0.0062	0.0131	0.0076	0.0202	0.0419	0.1705

Table 5: REL of the different method to solve Example 1 when the noise level is 0.05.

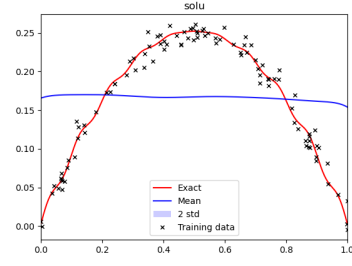
Initial step size(lr)	0.01	0.005	0.001	0.0005	0.0001	0.00005	0.00001
BPINN_HMC	—	—	—	—	—	0.3958	0.3979
FF_MBPINN_HMC	—	—	—	—	—	—	—
2FF_MBPINN_HMC	—	—	—	—	—	—	—
BPINN_SGD	0.3964	0.3962	0.3961	0.3987	0.3991	0.3995	0.3981
FF_MBPINN_SGD	0.0876	0.0663	0.0323	0.0223	0.0464	0.0747	0.6851
2FF_MBPINN_SGD	0.0174	0.0405	0.0201	0.0216	0.0257	0.0342	0.0911

Table 6: REL of the different method to solve Example 1 when the noise level is 0.1.

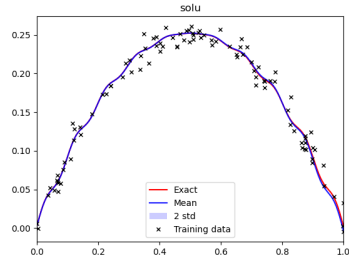
Initial step size(lr)	0.01	0.005	0.001	0.0005	0.0001	0.00005	0.00001
BPINN_HMC	—	—	—	—	0.4018	0.4016	0.3966
FF_MBPINN_HMC	—	—	—	—	—	—	—
2FF_MBPINN_HMC	—	—	—	—	—	—	—
BPINN_SGD	0.4025	0.4016	0.4018	0.4019	0.4017	0.4016	0.3986
FF_MBPINN_SGD	0.0980	0.1021	0.0431	0.0271	0.0225	0.0107	0.4926
2FF_MBPINN_SGD	0.1073	0.0125	0.0409	0.0505	0.0393	0.0288	0.0618



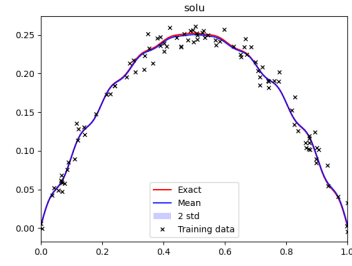
(a) BPINN_HMC



(b) BPINN_SGD

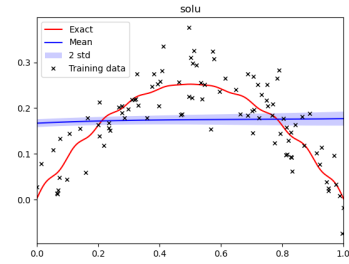


(c) FF_MBPINN_SGD

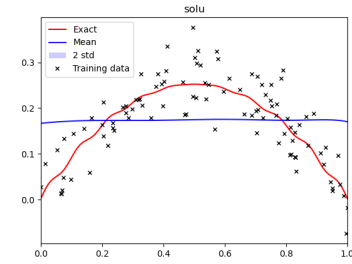


(d) 2FF_MBPINN_SGD

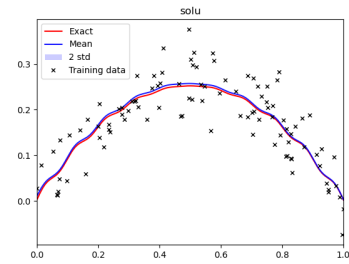
Figure 6: The exact and predicted solutions for Example 1 when the noise level is 0.01 .



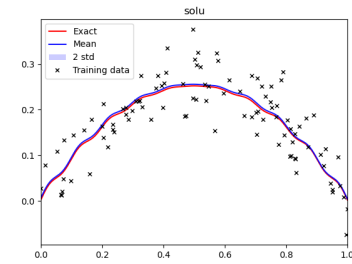
(a) BPINN_HMC



(b) BPINN_SGD



(c) FF_MBPINN_SGD



(d) 2FF_MBPINN_SGD

Figure 7: The exact and predicted solutions for Example 1 when the noise level is 0.05.

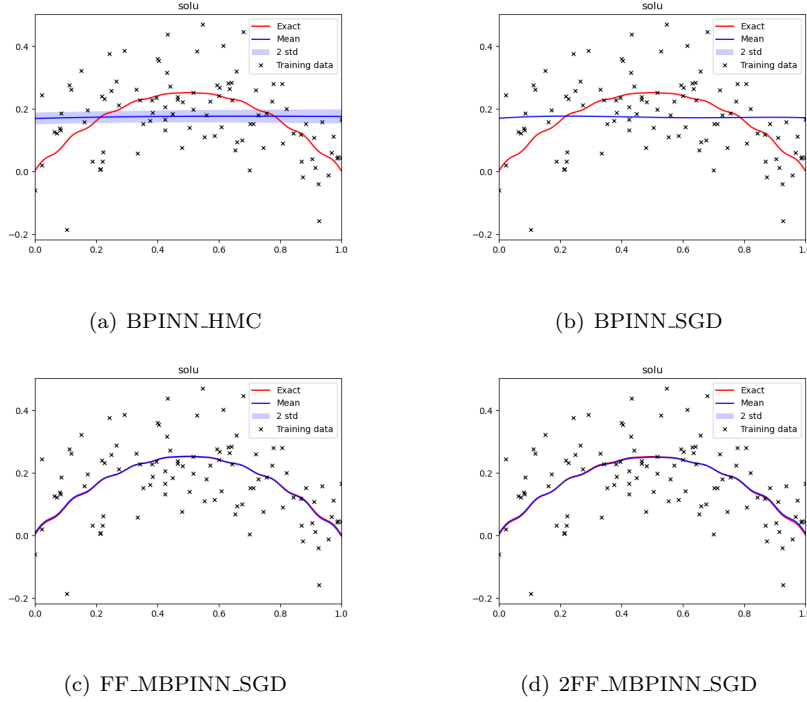


Figure 8: The exact and predicted solutions for Example 1 when the noise level is 0.1.

The results in Tables 4 – 6 and Figures 6 – 8 demonstrate that the FF MBPINN_SGD and 2FF MBPINN_SGD methods exceed the performance of the classical BPINN_HMC and BPINN_SGD methods when the HMC driven BPINN is worked. In addition, the performance of FF MBPINN_SGD is competed against that of 2FF MBPINN_SGD. It is important to note that when the FFM is introduced into the classical BPINN framework, the convergence issues associated with HMC become even more pronounced because of the FFM layer enlarges the effects of stepsize for HMC’s lepfrog.

Influence of the learning rate: We study the influence of decayed step size or learning rate for our proposed methods to solve the above two-scale elliptic problem when the $\varepsilon = 0.1$ and the noise level is 0.05. In the test, the initial value of step size or learning are set as 0.01, 0.005, 0.001, 0.0005, 0.0001, 0.00005 and 0.00001, respectively. In which, the learning rate will be decayed by 5% for every 100 training epochs and the step size will decay 5% for every 20 steps in our traing processes. Their other setups are identical to the above experiments. Based on the results in Table 7 and the results in Table 5, the decayed step size or learning rate is inferior to the fixed cases for the our proposed methods in solving multi-scale problems.

Table 7: REL of the different learning rates for the above methods to solve Example 1.

Initial step size(lr)	0.01	0.005	0.001	0.0005	0.0001	0.00005	0.00001
BPINN_HMC	—	—	—	—	—	0.3998	0.3981
FF_MBPINN_HMC	—	—	—	—	—	—	—
2FF_MBPINN_HMC	—	—	—	—	—	—	—
BPINN_SGD	0.3989	0.3993	0.3994	0.3991	0.3981	0.3981	0.3979
FF_MBPINN_SGD	0.1271	0.0747	0.0892	1.0366	6.1769	7.0061	6.3309
2FF_MBPINN_SGD	0.0202	0.0361	0.1851	0.2523	0.4349	1.5280	2.7352

Influence of the hidden units: We study the influence of hidden units including width and depth for our proposed methods to solve the aforementioned two-scale elliptic problem when the $\varepsilon = 0.1$ and the noise level is 0.05. In the test, the hidden units are set as (20, 20), (40, 40), (50, 50), (20, 20, 20), (30, 30, 30) and (40, 40, 40), respectively, except for the original configuration of hidden units. All other setups are identical to the aforementioned experiments, except for the step size or learning rate are fixed as 0.001. Based on the

results in Table 8, the performance for our proposed methods will be improved when the width of hidden layers increases from 20 to 40, but it will degrade for 50. Moreover, their performance are unstable for the cases of three hidden layers. This phenomenon reveals that the ability of Bayesian neural networks will become degenerated when the network parameters exceed the requirement[38].

Table 8: REL of different depth and width for hidden units when the above methods is used to solve Example 1.

Network size	(20, 20)	(30, 30)	(40, 40)	(50, 50)	(20, 20, 20)	(30, 30, 30)	(40, 40, 40)
BPINN_HMC	—	—	—	—	—	—	—
FF_MBPINN_HMC	—	—	—	—	—	—	—
2FF_MBPINN_HMC	—	—	—	—	—	—	—
BPINN_SGD	0.3983	0.3964	0.3977	0.3962	0.3959	0.3968	0.3946
FF_MBPINN_SGD	0.1332	0.0323	0.0268	0.0964	0.0232	0.0463	0.0213
2FF_MBPINN_SGD	0.0522	0.0201	0.0188	0.0419	0.0329	0.0218	0.0314

Influence of the number for noise observations: We study the influence of noise observations for our proposed methods to solve the above two-scale elliptic problem when the $\varepsilon = 0.1$ and the noise level is 0.05. Except for the existed 100 noisy observations for solution and force side, we further randomly sample 73 and 148 inner observations, respectively, and 2 boundary observations for solution, we then disturb them by the mean-zero Gaussian noise. As for the force side, 75 and 150 observations sampled randomly from Ω are also disturbed with mean-zero Gaussian distributed noise. The other setups are identical to the above experiments. Based on the results in Table 5 and Tables 9 – 10, we observe that the performance of BPINN_HMC keeps unchanged with the number of noisy observation increasing when it works successfully, but the FF_MBPINN_SGD and 2FF_MBPINN_SGD will be improved.

Table 9: The performance of different methods to solve Example 1 for 75 noise observations.

Initial step size(lr)	0.01	0.005	0.001	0.0005	0.0001	0.00005	0.00001
BPINN_HMC	—	—	—	—	—	0.4011	0.4054
FF_MBPINN_HMC	—	—	—	—	—	—	—
2FF_MBPINN_HMC	—	—	—	—	—	—	—
BPINN_SGD	—	—	—	—	—	—	—
FF_MBPINN_SGD	0.1789	0.1766	0.0554	0.0628	0.0673	0.0698	0.1145
2FF_MBPINN_SGD	0.2165	0.0773	0.0537	0.0457	0.0535	0.0536	0.1055

Table 10: The performance of different methods to solve Example 1 for 150 noise observations.

Initial step size(lr)	0.01	0.005	0.001	0.0005	0.0001	0.00005	0.00001
BPINN_HMC	—	—	—	—	—	0.4013	0.4023
FF_MBPINN_HMC	—	—	—	—	—	—	—
2FF_MBPINN_HMC	—	—	—	—	—	—	—
BPINN_SGD	—	—	—	—	—	—	—
FF_MBPINN_SGD	0.0825	0.0610	0.0499	0.0398	0.0494	0.0592	0.9216
2FF_MBPINN_SGD	0.1801	0.1205	0.0141	0.0194	0.0203	0.0208	0.1015

Example 2. Now, let us study the performance for our proposed MBPINN method to the general problems. We consider the following non-linear Poisson problem with two frequency components in $\Omega = [0, 1]$:

$$\begin{cases} 0.01\Delta u(x) + k(x)u(x) = f(x) \\ u(0) = u(1) = 0.1. \end{cases} \quad (4.1)$$

with a coefficient term $k(x)$ as follows

$$k(x) = 0.1 + \exp\left(-0.5 \frac{(x - 0.5)^2}{0.15^2}\right) \quad (4.2)$$

An exact solution is given by

$$u_{\text{true}}(x) = \sin(2\pi x) + 0.1 \cos(10\pi x) \quad (4.3)$$

it naturally induces the force term

$$f(x) = 0.01 (-4\pi^2 \sin(2\pi x) - 10\pi^2 \cos(10\pi x)) + k(x) \cdot u(x). \quad (4.4)$$

We solve the above problem by employing the aforementioned six methods that their solvers have two hidden layers and each layer has 30 units. In this example, 50 observations sampled randomly from Ω for the solution and force side, respectively, are disturbed with mean-zero Gaussian distributed noise. In addition, the 25 observations sampled randomly from Ω for the coefficient term, $k(x)$, are disturbed as well. To recover the solution and coefficient term simultaneously, two ansatzes expressed by DNN are used in BPINN method, and two ansatzes expressed by MscaledDNN with FFM pipelines are used in other methods. The standard deviation for Λ of FF_MBPINN is set as 5 and 0.5 for solution and coefficient, respectively. The standard deviations for Λ_1 and Λ_2 of 2FF_MBPINN used to expressed solution are set as 1 and 5, but for coefficient are set as 0.1 and 0.5, respectively. Additionally, the SNRs for solution, coefficient term and force side are 22.3147, 20.2577 and 23.2779, respectively, when the noise level is 0.05. Finally, we list and depict the related experiment results in Tables 11 – 12 and Figures 9 – 10, respectively.

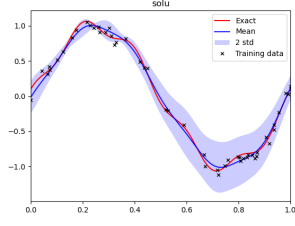
Table 11: REL of solution for different methods to solve Example 2 when the noise level is 0.05.

Initial step size(lr)	0.01	0.005	0.001	0.0005	0.0001	0.00005	0.00001
BPINN_HMC	—	—	—	—	0.0715	0.1176	0.6259
FF_MBPINN_HMC	—	—	—	—	0.0253	0.0228	0.0559
2FF_MBPINN_HMC	—	—	—	—	0.0261	0.0305	0.0626
BPINN_SGD	0.0279	0.0266	0.0248	0.0234	0.2940	0.1133	0.6066
FF_MBPINN_SGD	0.0251	0.0247	0.0238	0.0249	0.0248	0.0250	0.0285
2FF_MBPINN_SGD	0.0257	0.0276	0.0261	0.0261	0.0260	0.0252	0.0292

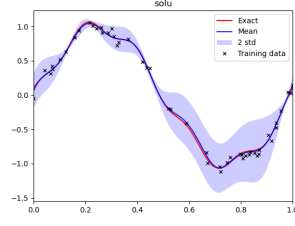
Table 12: REL of parameter for different methods to solve Example 2 when the noise level is 0.05.

Initial step size(lr)	0.01	0.005	0.001	0.0005	0.0001	0.00005	0.00001
BPINN_HMC	—	—	—	—	0.2361	0.3379	0.8291
FF_MBPINN_HMC	—	—	—	—	0.0482	0.0679	0.2688
2FF_MBPINN_HMC	—	—	—	—	0.0491	0.0985	0.3334
BPINN_SGD	0.0668	0.0410	0.0605	0.0487	1.6010	0.4244	0.6420
FF_MBPINN_SGD	0.0477	0.0394	0.0380	0.0379	0.0380	0.0375	0.0942
2FF_MBPINN_SGD	0.0422	0.0510	0.0476	0.0478	0.0457	0.0466	0.1013

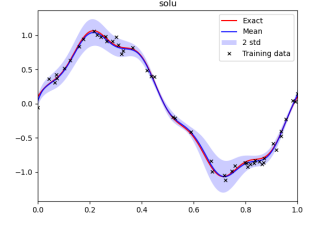
From the results in Tables 11 – 12 and Figs. 9 – 10, the FF_MBPINN and 2FF_MBPINN method are superior to the classical BPINN in terms of the same step size or learning rate. In which, BPINN_HMC method fails to work when the step size is relatively large and its performance will be deteriorated with the noise level increasing when it is successful to work. Although the MBPINN_HMC and 2FF_MBPINN_HMC methods also face the issues with failure, they perform better when they succeeds in working. It is important to note that a plus of the MBPINN_HMC method is its ability to provide interval estimates for parameters, whereas MBPINN_SGD only offers point estimates. Moreover, the SGD driven BPINN, FF_MBPINN and 2FF_MBPINN outperform the HMC driven ones, and they can provide the satisfactory point estimation for the interval parameters. Additionally, the performance of FF_MBPINN and 2ff_MBPINN method are completed. In conclusion, the MBPINN_SGD method consistently provides the best point estimates for parameters and reliably produces results.



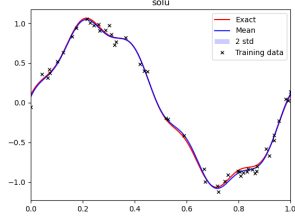
(a) BPINN_HMC



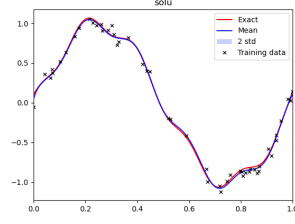
(b) FF_MBPINN_HMC



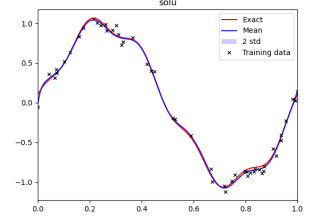
(c) 2FF_MBPINN_HMC



(d) BPINN_SGD

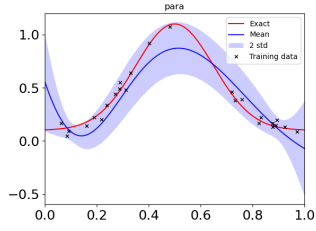


(e) FF_MBPINN_SGD

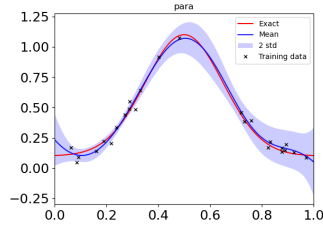


(f) 2FF_MBPINN_SGD

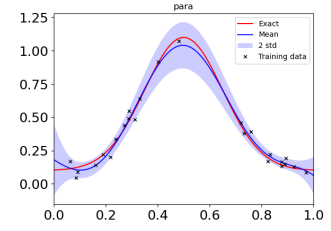
Figure 9: Visualization of the solution for different methods to solve Example 2 when the noise level is 0.05.



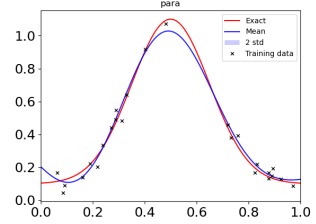
(a) BPINN_HMC



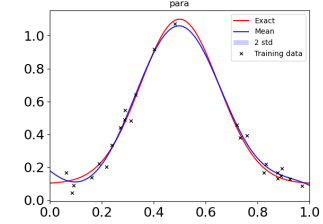
(b) FF_MBPINN_HMC



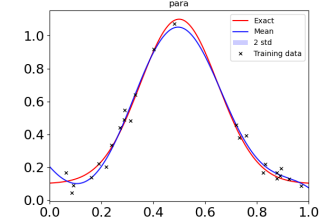
(c) 2FF_MBPINN_HMC



(d) BPINN_SGD



(e) FF_MBPINN_SGD



(f) 2FF_MBPINN_SGD

Figure 10: Visualization of the parameter for different methods to solve Example 2 when the noise level is 0.05.

4.2. Performance of MBPINN for Solving two-dimensional PDEs

Example 3. Now, our goal is to deal with the following multiscale elliptic equation in a regular rectangle domain $\Omega = [0, 1] \times [0, 1]$.

$$\begin{cases} -\operatorname{div}(A^\varepsilon(x_1, x_2)\nabla u^\varepsilon(x_1, x_2)) = f(x_1, x_2) \\ u^\varepsilon(x_1, 0) = \frac{1}{4}x_1^4 + \frac{\varepsilon}{16}x_1^2 \sin\left(\frac{2\pi x_1^2}{\varepsilon}\right) + \frac{\varepsilon^2}{32\pi^2} \cos\left(\frac{2\pi x_1^2}{\varepsilon}\right) \\ u^\varepsilon(x_1, 1) = \frac{1}{4}(x_1^2 + 1)^2 + \frac{\varepsilon}{16}(x_1^2 + 1) \sin\left(\frac{2\pi(1 + x_1^2)}{\varepsilon}\right) + \frac{\varepsilon^2}{32\pi^2} \cos\left(\frac{2\pi(x_1^2 + 1)}{\varepsilon}\right) \\ u^\varepsilon(0, x_2) = \frac{1}{4}x_2^4 + \frac{\varepsilon}{16}x_2^2 \sin\left(\frac{2\pi x_2^2}{\varepsilon}\right) + \frac{\varepsilon^2}{32\pi^2} \cos\left(\frac{2\pi x_2^2}{\varepsilon}\right) \\ u^\varepsilon(1, x_2) = \frac{1}{4}(1 + x_2^2)^2 + \frac{\varepsilon}{16}(1 + x_2^2) \sin\left(\frac{2\pi(1 + x_2^2)}{\varepsilon}\right) + \frac{\varepsilon^2}{32\pi^2} \cos\left(\frac{2\pi(1 + x_2^2)}{\varepsilon}\right) \end{cases} \quad (4.5)$$

in which

$$A^\varepsilon(x_1, x_2) = \frac{1}{4 + \cos\left(\frac{2\pi(x_1^2 + x_2^2)}{\varepsilon}\right)}, \quad (4.6)$$

with $\varepsilon > 0$ being a small constant and $f(x_1, x_2) = -(x_1^2 + x_2^2)$. Under these conditions, an exact solution is given by

$$u^\varepsilon(x_1, x_2) = \frac{1}{4}(x_1^2 + x_2^2)^2 + \frac{\varepsilon}{16\pi}(x_1^2 + x_2^2) \sin\left(\frac{2\pi(x_1^2 + x_2^2)}{\varepsilon}\right) + \frac{\varepsilon^2}{32\pi^2} \cos\left(\frac{2\pi(x_1^2 + x_2^2)}{\varepsilon}\right). \quad (4.7)$$

We utilize the aforementioned six methods to solve the above two-dimensional multiscale elliptic problem with $\varepsilon = 0.5$ when the noise level is 0.01 and 0.02, respectively. Their solvers all have two hidden layers and each layer has 40 neuron units. In this example, we randomly sample 500 observations for force side in Ω and disturb them by Gaussian distribution noise with zero mean error. In addition, 500 random observations composed of 400 interior points and 100 boundary points for solution in Ω are disturbed as well. To recover the solution from these noise observations, an ansatz expressed by DNN is used in BPINN method and an ansatz expressed by MscaledDNN with FFM pipelines is used in other methods. The standard deviation of Λ for FF_MBPINN is set as 5 and the standard deviations of Λ_1 and Λ_2 for 2FF_MBPINN are set as 1 and 5, respectively. We list and plot the related experiment results in Tables 13 – 15 and Figure 12, respectively.

Table 13: SNR of solution and force side under various noise level for Example 3.

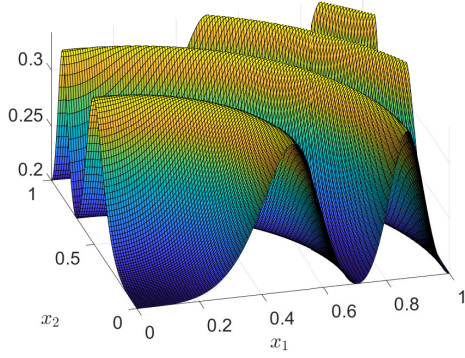
Noise level	0.01	0.02
solution	28.117	22.763
force side	37.963	31.653

Table 14: REL of solution for different methods to solve Example 3 when the noise level is 0.01.

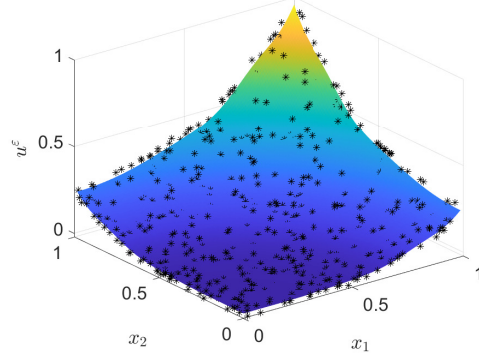
Initial step size(lr)	0.01	0.005	0.001	0.0005	0.0001	0.00005	0.00001
BPINN_HMC	—	—	—	—	0.7008	0.9686	1.0734
FF_MBPINN_HMC	—	—	—	—	—	—	—
2FF_MBPINN_HMC	—	—	—	—	—	—	—
BPINN_SGD	0.0530	0.0733	0.8672	0.9507	0.9662	0.9673	1.0768
FF_MBPINN_SGD	0.1329	0.0426	0.0748	0.0889	0.1323	0.1537	0.4266
2FF_MBPINN_SGD	0.0690	0.0201	0.1441	0.1887	0.2375	0.2596	0.4843

Table 15: REL of solution for different methods to solve Example 3 when the noise level is 0.02.

Initial step size(lr)	0.01	0.005	0.001	0.0005	0.0001	0.00005	0.00001
BPINN_HMC	—	—	—	—	0.9136	0.9278	0.8566
FF_MBPINN_HMC	—	—	—	—	—	—	—
2FF_MBPINN_HMC	—	—	—	—	—	—	—
BPINN_SGD	0.0397	0.0847	0.6415	0.8368	0.9082	0.9089	0.9755
FF_MBPINN_SGD	0.0481	0.0351	0.0863	0.0941	0.1250	0.1470	0.4315
2FF_MBPINN_SGD	0.1189	0.0299	0.1391	0.1743	0.2075	0.2233	0.4471

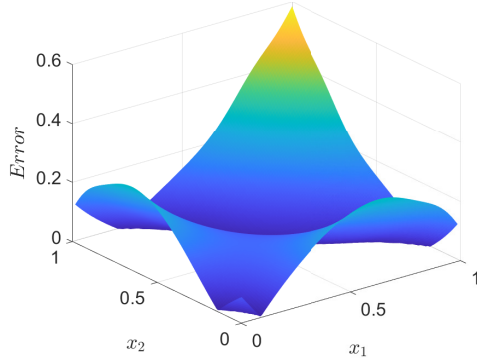


(a) $A^\epsilon(x_1, x_2)$

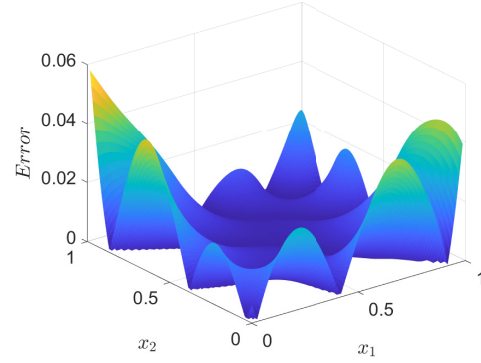


(b) Exact solution and noisy observations

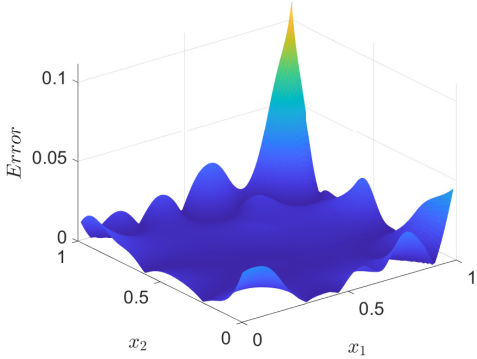
Figure 11: Coefficient and exact solution with noisy observations for Example 3.



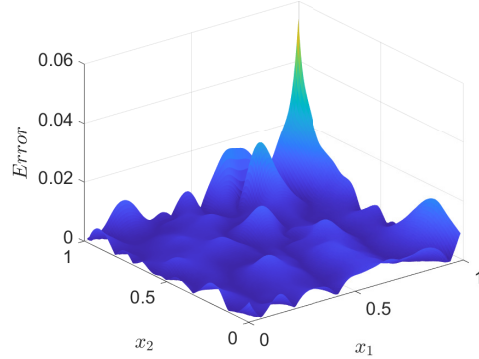
(a) BPINN_HMC for step size=0.0005



(b) MBPINN_SGD for lr=0.005



(c) FF_MBPINN_SGD for lr=0.005



(d) 2FF_MBPINN_SGD for lr=0.005

Figure 12: The point-wise error of numerical methods for Example 3 when the noise level is 0.01

Based the point-wise errors in Figure 12 and the relative error in Tables 13 – 15, we can conclude that the both FF_MBPINN_SGD and 2FF_MBPINN_SGD outperform the other methods, especially at smaller step sizes, when these methods are successful to work. It is important to note that the HMC driven MBPINN methods are not able to provide the solution for our problem. The BPINN_HMC method works and provides a result under the small step size, but its performance is terrible. This indicates that the result was entirely dependent on the initialization and their performance is affected by the step size used to update the interval parameters of solver, in particularly for multi-scale PDEs. This highlights a critical limitation of this method for the utilization to the multi-scale scenario and indicates the superiority of SGD technique.

Example 4. Now, our goal is to deal with the following general Poisson equation in a regular rectangle domain $\Omega = [-1, 1] \times [-1, 1]$.

$$\begin{cases} \Delta u(x_1, x_2) = f(x_1, x_2) \\ u(-1, y) = u(1, y) = e^{\sin(\pi x_2)} \\ u(x, -1) = u(x, 1) = e^{\sin(\pi x_1)}. \end{cases} \quad (4.8)$$

An exact solution is given by

$$u(x_1, x_2) = e^{\sin(\pi x_1)} e^{\sin(\pi x_2)} \quad (4.9)$$

such that

$$f(x_1, x_2) = \pi^2 e^{\sin(\pi x_1)} e^{\sin(\pi x_2)} [\cos^2(\pi x_1) - \sin(\pi x_1) + \cos^2(\pi x_2) - \sin(\pi x_2)]$$

We solve the above smooth Poisson problem by employing the aforementioned six methods when the noise level is 0.2. In this example, we randomly sample 800 random observations for force side and solution in Ω , respectively. We then disturb these observations by Gaussian distributed noise with zero mean error. In addition, the standard deviation of Λ for FF_MBPINN is set as 1.0 and the standard deviations of Λ_1 and Λ_2 for 2FF_MBPINN are set as 0.2 and 1.0, respectively. The all setups are same as the above Example 3. In our test, the SNRs for solution and force side are 20.538 and 43.587, respectively. We list and depict the related experiment results in Table 16 and Figure 14, respectively.

Table 16: REL of different method with two hidden layers to solve Example 4 when the noise is 0.2.

Initial step Size(lr)	0.01	0.005	0.001	0.0005	0.0001	0.00005	0.00001
BPINN_HMC	—	—	—	—	—	0.0107	0.0343
FF_MBPINN_HMC	—	—	—	—	—	—	0.0294
2FF_MBPINN_HMC	—	—	—	—	—	—	0.0381
BPINN_SGD	0.0130	0.0127	0.0203	0.0186	0.0272	0.0497	0.5835
FF_MBPINN_SGD	0.0102	0.0110	0.0097	0.0095	0.0094	0.0099	0.0647
2FF_MBPINN_SGD	0.0186	0.0121	0.0105	0.0106	0.0116	0.0131	0.0613

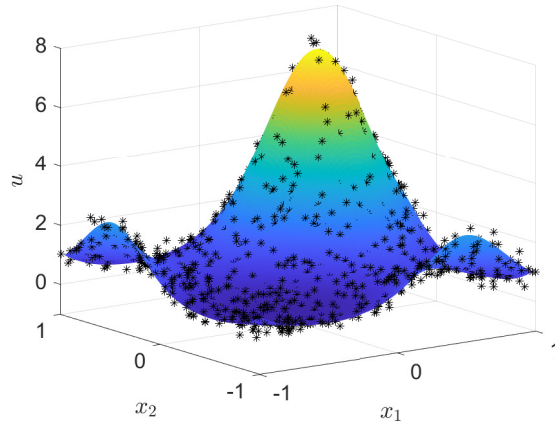


Figure 13: Exact solution and noisy observations for Example 4.

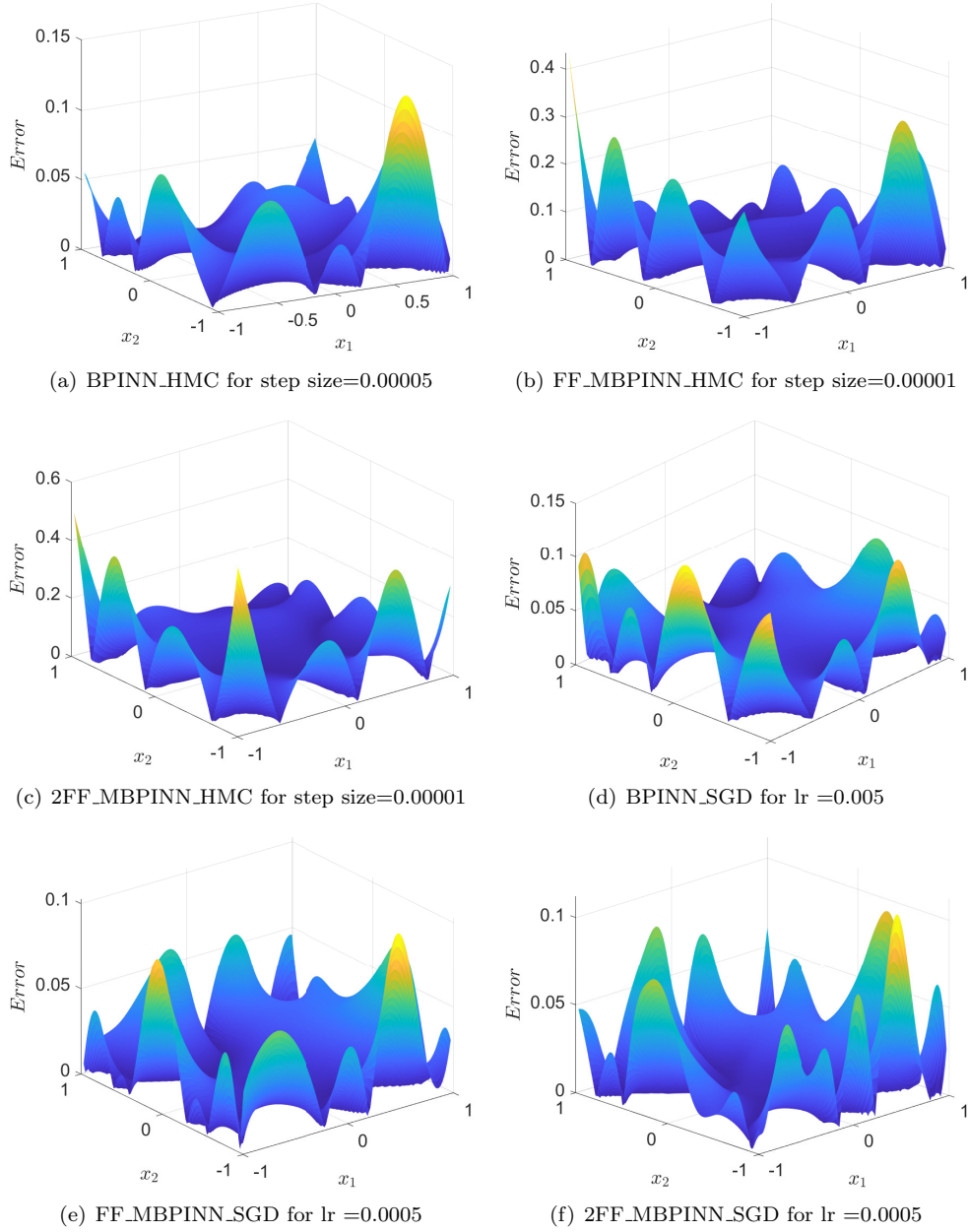


Figure 14: The point-wise error of numerical methods for Example 3 when noise level is 0.05

The results in Table 16 and the point wise absolute error in Figure 14 indicate that the SGD driven BPINN and MBPINN methods are generally superior to the HMC-based ones when they are successful to solve this problem. Furthermore, the use of SGD proves to be more effective in reducing errors, especially at moderate step sizes, demonstrating that even in two-dimensional settings, SGD-based methods remain effective and robust. It is important to note that SGD-based methods have significantly lower computational costs compared to HMC-based methods, a difference that becomes even more pronounced in two-dimensional problems. In addition, the failure of convergence for HMC estimation method with large step size is still occurred when classical BPINN and our proposed method are used to resolve this general Poisson problem in two dimensional space, in particular for our proposed methods. Under this case, our proposed methods

still outperform the BPINN method.

5. Conclusion

The classical BPINN method faces significant challenges in practical applications, particularly due to the convergence issues of the HMC sampling method when solving general elliptic PDEs, which are exacerbated as the complexity of the PDEs increases. Additionally, the basic setup of BPINN is somewhat simplistic and performs poorly when the complexity of PDEs increases and the step size used to update the solver’s interval parameters is large. To address these issues simultaneously, we propose an enhanced BPINN by incorporating a FFM induced multi-scale DNN into this architecture, which has been tested and compared against BPINN method on general Poisson across one and two-dimensional spaces with noisy data. Moreover, we reframe the estimation approach for the interval parameters of this proposed novel method in terms of the failure of the HMC caused by the step size and the complexity of PDE problems, especially for multi-scale elliptic PDEs. Our results demonstrate that the SGD driven MBPINN (1) is more robust than HMC, (2) incurs lower computational costs, and (3) offers greater flexibility in handling complex problems. However, when MBPINN is combined with HMC, the convergence issues of HMC worsen due to the inherent complexity of the neural network solver and the problem to be solved, a challenge that warrants further investigation in the future.

Credit authorship contribution Statement

Yilong Hou: Methodology, Investigation, Formal analysis, Validation, Writing - Original Draft. Xi’an Li: Conceptualization, Methodology, Investigation, Formal analysis, Validation, Writing - Review & Editing. Jinran Wu: Formal analysis, Writing - Review & Editing. You-Gan Wang: Writing - Review & Editing, Project administration.

Acknowledgements

This study was supported by the Natural Science Foundation of Shandong Province, China (No.ZR2024QF057).

References

- [1] A. Pensoneault, X. Zhu, Efficient bayesian physics informed neural networks for inverse problems via ensemble kalman inversion, *Journal of Computational Physics* 508 (2024) 113006.
- [2] H. W. Engl, M. Hanke, A. Neubauer, *Regularization of inverse problems*, volume 375, Springer Science & Business Media, 1996.
- [3] J. V. Beck, K. J. Arnold, *Parameter estimation in engineering and science*, James Beck, 1977.
- [4] K. A. Woodbury, *Inverse engineering handbook*, Crc press, 2002.
- [5] J. Wang, N. Zabaras, Hierarchical bayesian models for inverse problems in heat conduction, *Inverse Problems* 21 (2004) 183.
- [6] L. Yang, X. Meng, G. E. Karniadakis, B-pinns: Bayesian physics-informed neural networks for forward and inverse pde problems with noisy data, *Journal of Computational Physics* 425 (2021) 109913.
- [7] M. Yang, J. T. Foster, Multi-output physics-informed neural networks for forward and inverse pde problems with uncertainties, *Computer Methods in Applied Mechanics and Engineering* 402 (2022) 115041.
- [8] K. Linka, A. Schäfer, X. Meng, Z. Zou, G. E. Karniadakis, E. Kuhl, Bayesian physics informed neural networks for real-world nonlinear dynamical systems, *Computer Methods in Applied Mechanics and Engineering* 402 (2022) 115346.
- [9] J. Li, Y. M. Marzouk, Adaptive construction of surrogates for the bayesian solution of inverse problems, *SIAM Journal on Scientific Computing* 36 (2014) A1163–A1186.
- [10] R. M. Neal, *Bayesian learning for neural networks*, volume 118, Springer Science & Business Media, 2012.
- [11] J. Lee, Y. Bahri, R. Novak, S. S. Schoenholz, J. Pennington, J. Sohl-Dickstein, Deep neural networks as gaussian processes, *arXiv preprint arXiv:1711.00165* (2017).
- [12] M. Betancourt, The convergence of markov chain monte carlo methods: from the metropolis method to hamiltonian monte carlo, *Annalen der Physik* 531 (2019) 1700214.
- [13] R. M. Neal, et al., Mcmc using hamiltonian dynamics, *Handbook of markov chain monte carlo* 2 (2011) 2.
- [14] M. Betancourt, A conceptual introduction to hamiltonian monte carlo, *arXiv preprint arXiv:1701.02434* (2017).

- [15] D. M. Blei, A. Kucukelbir, J. D. McAuliffe, Variational inference: A review for statisticians, *Journal of the American statistical Association* 112 (2017) 859–877.
- [16] A. Y. Foong, Y. Li, J. M. Hernández-Lobato, R. E. Turner, 'In-Between' Uncertainty in Bayesian Neural Networks, *arXiv preprint arXiv:1906.11537* (2019).
- [17] J. Yao, W. Pan, S. Ghosh, F. Doshi-Velez, Quality of uncertainty quantification for Bayesian neural network inference, *arXiv preprint arXiv:1906.09686* (2019).
- [18] D. Ceccarelli, Bayesian physics-informed neural networks for inverse uncertainty quantification problems in cardiac electrophysiology, Milan, Italy: Polytechnic Univ. Milan (2021).
- [19] P. Li, D. Grana, M. Liu, Bayesian neural network and bayesian physics-informed neural network via variational inference for seismic petrophysical inversion, *Geophysics* 89 (2024) 1–46.
- [20] H. Antil, H. C. Elman, A. Onwunta, D. Verma, Novel deep neural networks for solving bayesian statistical inverse, *arXiv preprint arXiv:2102.03974* (2021).
- [21] G. Lin, Y. Wang, Z. Zhang, Multi-variance replica exchange sgcmc for inverse and forward problems via bayesian pinn, *Journal of Computational Physics* 460 (2022) 111173.
- [22] Y. Li, Y. Wang, L. Yan, Surrogate modeling for bayesian inverse problems based on physics-informed neural networks, *Journal of Computational Physics* 475 (2023) 111841.
- [23] L. Sun, J.-X. Wang, Physics-constrained bayesian neural network for fluid flow reconstruction with sparse and noisy data, *Theoretical and Applied Mechanics Letters* 10 (2020) 161–169.
- [24] X. Jiang, X. Wang, Z. Wena, E. Li, H. Wang, An E-PINN assisted practical uncertainty quantification for inverse problems, *arXiv preprint arXiv:2209.10195* (2022).
- [25] M. A. Iglesias, K. J. Law, A. M. Stuart, Ensemble kalman methods for inverse problems, *Inverse Problems* 29 (2013) 045001.
- [26] X. Meng, L. Yang, Z. Mao, J. del Águila Ferrandis, G. E. Karniadakis, Learning functional priors and posteriors from data and physics, *Journal of Computational Physics* 457 (2022) 111073.
- [27] S. Perez, S. Maddu, I. F. Sbalzarini, P. Poncet, Adaptive weighting of bayesian physics informed neural networks for multitask and multiscale forward and inverse problems, *Journal of Computational Physics* 491 (2023) 112342.
- [28] Z.-Q. J. Xu, Y. Zhang, T. Luo, Y. Xiao, Z. Ma, Frequency principle: Fourier analysis sheds light on deep neural networks, *Communications in Computational Physics* 28 (2020) 1746–1767.
- [29] N. Rahaman, D. Arpit, A. Baratin, F. Draxler, M. Lin, F. A. Hamprecht, Y. Bengio, A. Courville, On the spectral bias of deep neural networks, *International Conference on Machine Learning* (2019).
- [30] S. Wang, H. Wang, P. Perdikaris, On the eigenvector bias of Fourier feature networks: From regression to solving multi-scale PDEs with physics-informed neural networks, *Computer Methods in Applied Mechanics and Engineering* 384 (2021) 113938.
- [31] M. Tancik, P. Srinivasan, B. Mildenhall, S. Fridovich-Keil, N. Raghavan, U. Singhal, R. Ramamoorthi, J. Barron, R. Ng, Fourier features let networks learn high frequency functions in low dimensional domains, *Advances in Neural Information Processing Systems* 33 (2020) 7537–7547.
- [32] S. Li, Y. Xia, Y. Liu, Q. Liao, A deep domain decomposition method based on Fourier features, *Journal of Computational and Applied Mathematics* 423 (2023) 114963.
- [33] Y. Zong, D. Barajas-Solano, A. M. Tartakovsky, Randomized physics-informed neural networks for bayesian data assimilation, *Computer Methods in Applied Mechanics and Engineering* 436 (2025) 117670.
- [34] Z. Liu, W. Cai, Z.-Q. J. Xu, Multi-scale Deep Neural Network (MscaleDNN) for Solving Poisson-Boltzmann Equation in Complex Domains, *Communications in Computational Physics* 28 (2020) 1970–2001.
- [35] B. Wang, W. Zhang, W. Cai, Multi-Scale Deep Neural Network (MscaleDNN) Methods for Oscillatory Stokes Flows in Complex Domains, *Communications in Computational Physics* 28 (2020) 2139–2157.
- [36] Y. Wang, Y. Yao, J. Guo, Z. Gao, A practical pinn framework for multi-scale problems with multi-magnitude loss terms, *Journal of Computational Physics* 510 (2024) 113112.
- [37] X.-A. Li, Z.-Q. J. Xu, L. Zhang, Subspace decomposition based DNN algorithm for elliptic type multi-scale PDEs, *Journal of Computational Physics* (2023) 112242.
- [38] Z. John Lu, *The elements of statistical learning: data mining, inference, and prediction*, 2010.

Appendix A: Hamiltonian Monte Carlo (HMC)

Hamiltonian Monte Carlo (HMC) augment the parameter space $\boldsymbol{\theta}$ into $(\boldsymbol{\theta}, \mathbf{r})$ with an auxiliary momentum variable \mathbf{r} , which matches the dimensionality of $\boldsymbol{\theta}$. This formulation enables the use of Hamiltonian dynamics to propose new states in the phase space, facilitating efficient exploration of the posterior distribution. The Hamiltonian $H(\boldsymbol{\theta}, \mathbf{r})$ is composed of the potential energy $U(\boldsymbol{\theta})$, derived from the negative log-posterior, and the kinetic energy $K(\mathbf{r})$, often modeled as $\mathbf{r}^\top M^{-1} \mathbf{r} / 2$, where M is the mass matrix. By leveraging the continuous evolution of the Hamiltonian system, HMC avoids random-walk behavior and achieves faster convergence compared to traditional sampling methods.

The process begins by sampling an initial momentum $\mathbf{r}_0 \sim \mathcal{N}(0, M)$ and setting the initial states $(\boldsymbol{\theta}_0, \mathbf{r}_0)$ to the previous iteration's values $(\boldsymbol{\theta}^{t^{k-1}}, \mathbf{r}^{t^{k-1}})$. To simulate the Hamiltonian dynamics, the leapfrog inte-

grator is employed for L steps with a fixed step size d . The updates for momentum and parameters at each step follow these equations:

$$\begin{aligned} \mathbf{r}_i &\leftarrow \mathbf{r}_i - \frac{d}{2} \nabla U(\boldsymbol{\theta}_i), \\ \boldsymbol{\theta}_{i+1} &\leftarrow \boldsymbol{\theta}_i + dM^{-1}\mathbf{r}_i, \\ \mathbf{r}_{i+1} &\leftarrow \mathbf{r}_i - \frac{d}{2} \nabla U(\boldsymbol{\theta}_{i+1}). \end{aligned}$$

After completing L leapfrog steps, the Metropolis-Hastings acceptance criterion is applied. The acceptance probability α is given by:

$$\alpha = \min \left\{ 1, \exp(H(\boldsymbol{\theta}_L, \mathbf{r}_L) - H(\boldsymbol{\theta}^{t^{k-1}}, \mathbf{r}^{t^{k-1}})) \right\}.$$

$\boldsymbol{\theta}^L$ is accepted to be $\boldsymbol{\theta}^{t^k}$ with probability α ; otherwise, the previous state $\boldsymbol{\theta}^{t^{k-1}}$ is retained. The last few samples will be used for posterior inferences, which is a hyperparameter for user's choice.

The implementation code for HMC can be found at <https://github.com/AdamCobb/hamiltorch>, and the corresponding codes for estimating the parameters of a given neural network are as follows.

```
def params_grad(para):
    para = para.detach().requires_grad_()
    log_prob = log_prob_func(para)
    para = collect_gradients(log_prob, para, pass_grad)
    if torch.cuda.is_available():
        torch.cuda.empty_cache()
    return para.grad
ret_params = []
ret_momenta = []
momentum += 0.5 * step_size * params_grad(params)
for n in range(steps):
    if inv_mass is None:
        params = params + step_size * momentum
    else:
        if type(inv_mass) is list:
            i = 0
            for block in inv_mass:
                it = block[0].shape[0]
                params[i:it+i] = params[i:it+i] + step_size *
                    torch.matmul(block, momentum[i:it+i].view(-1,1)).view(-1)
                i += it
            elif len(inv_mass.shape) == 2:
                params = params + step_size * torch.matmul(inv_mass, momentum.view(-1,1)).view(-1)
            else:
                params = params + step_size * inv_mass * momentum
        p_grad = params_grad(params)
        momentum += step_size * p_grad
        ret_params.append(params.clone())
        ret_momenta.append(momentum.clone())
ret_momenta[-1] = ret_momenta[-1] - 0.5 * step_size * p_grad.clone()
```

```
def log_prob_func(params):
    params_unflattened = util.unflatten(model, params)
    i_prev = 0
    l_prior = torch.zeros_like(params[0], requires_grad=True)
    for weights, index, shape, dist in zip(model.parameters(), params_flattened_list,
```

```

        params_shape_list, dist_list):
    w = params[i_prev:index+i_prev]
    l_prior = dist.log_prob(w).sum() + l_prior
    i_prev += index

if x is None:
    return l_prior/prior_scale

x_device = x.to(device)
y_device = y.to(device)

output = fmodel(x_device, params=params_unflattened)

if model_loss == 'binary_class_linear_output':
    crit = nn.BCEWithLogitsLoss(reduction='sum')
    ll = - tau_out *(crit(output, y_device))
elif model_loss == 'multi_class_linear_output':
    crit = nn.CrossEntropyLoss(reduction='sum')
    ll = - tau_out *(crit(output, y_device.long().view(-1)))
elif model_loss == 'multi_class_log_softmax_output':
    ll = - tau_out *(torch.nn.functional.nll_loss(output, y_device.long().view(-1)))
elif model_loss == 'regression':
    ll = - 0.5 * tau_out * ((output - y_device) ** 2).sum(0)

elif callable(model_loss):
    ll = - model_loss(output, y_device).sum(0)
else:
    raise NotImplementedError()

if torch.cuda.is_available():
    del x_device, y_device
    torch.cuda.empty_cache()

if predict:
    return (ll + l_prior/prior_scale), output
else:
    return (ll + l_prior/prior_scale)

```
